



HAL
open science

Simple far-field radiative thermal rectifier using Fabry–Perot cavities based infrared selective emitters

E. Nefzaoui, Jérémie Drevillon, Y Ezzahri, Karl Joulain

► **To cite this version:**

E. Nefzaoui, Jérémie Drevillon, Y Ezzahri, Karl Joulain. Simple far-field radiative thermal rectifier using Fabry–Perot cavities based infrared selective emitters. *Applied optics*, 2014, 53 (16), pp.3479-3485. 10.1364/AO.53.003479 . hal-01543647

HAL Id: hal-01543647

<https://hal.science/hal-01543647v1>

Submitted on 30 Aug 2017

HAL is a multi-disciplinary open access archive for the deposit and dissemination of scientific research documents, whether they are published or not. The documents may come from teaching and research institutions in France or abroad, or from public or private research centers.

L'archive ouverte pluridisciplinaire **HAL**, est destinée au dépôt et à la diffusion de documents scientifiques de niveau recherche, publiés ou non, émanant des établissements d'enseignement et de recherche français ou étrangers, des laboratoires publics ou privés.

A simple far-field radiative thermal rectifier using Fabry-Pérot cavities based infrared selective emitters

E. Nefzaoui,^{1,*} J. Drevillon,² Y. Ezzahri,² and K. Joulain^{2,†}

¹*Université de Lyon, CNRS, INSA-Lyon, UCBL, CETHIL, UMR5008, Bât. Sadi-Carnot, Bur. 304B - INSA de Lyon 9,*

Rue de la physique - Campus La Doua F-69 621 Villeurbanne cedex, France

²*Institut Pprime, CNRS-Université de Poitiers-ENSMA, Département Fluides, Thermique, Combustion, ENSIP-Bâtiment de mécanique, 2, Rue Pierre Brousse, F 86022 Poitiers, Cedex, France*

Abstract

We present a thermal rectification device concept based on far-field radiative exchange between two selective emitters. Rectification is achieved due to a large contrast between the two selective emitters thermo-optical properties. A simple device constituted by two multilayer samples made of metallic (Au) and semiconductor (Si and HDSi) thin films is proposed. This device shows a rectification ratio increasing with temperature up to 19% for a temperature difference $\Delta T = 370$ K. Further optimization would allow larger rectification values. Presented results might be useful for energy conversion devices, smart radiative coolers / insulators engineering and thermal logical circuits development.

OCIS codes: 290.6815 Thermal emission, 050.2230 Fabry-Perot, 140.6810 Thermal effects, 160.6840

Thermo-optical materials

<http://dx.doi.org/10.1364/XX.99.099999>

* elyes.nefzaoui@univ-poitiers.fr

† karl.joulain@univ-poitiers.fr

1. Introduction

Thermal rectification can be defined as an asymmetry in the heat flux when the temperature difference between two interacting thermal reservoirs is reversed. The realization of a device exhibiting such an uncommon behaviour, a thermal rectifier for instance, would pave the way to the development of thermal circuits in the manner non-linear electronic devices marked the genesis of modern electronics[1]. Indeed, as in electronics, thermal logical circuits need a thermal diode which can be defined as an ideal rectifier, *i.e.* a one-way heat transmitter.

Consequently, an increasing interest has been given to thermal rectifiers during the last years. Experimental rectifiers based on carbon and boron nitride nanotubes [2], semiconductor quantum dots [3] and bulk cobalt oxides[4] were realized. Furthermore, numerous theoretical models were proposed, based on non-linear lattices [5–8], graphene nano-ribbons [9, 10] and several other interesting mechanisms [11, 12]. Some authors went beyond the thermal rectifiers issue and proposed theoretical models of thermal logical gates [13] and a thermal transistor [14]. An overwhelming majority of the proposed devices schemes were based on conductive heat transfer channels control. Extensive reviews treating thermal rectification in solids can be found in Refs. [15, 16].

In spite of this growing attention, very scarce radiative thermal rectifiers have been reported thus far. Indeed, a theoretical study and an experimental suggestion of a radiative thermal rectifier based on non-linear solid-state quantum circuits operating at very low temperatures (a few mK) were recently presented [17]. A rectification up to 10% was predicted. Moreover, theoretical schemes of radiative thermal rectification based on near-field thermal radiation control between different materials were lately proposed [18–21]. A rectification up to 30% (according to the present paper rectification definition and using the references data) was theoretically predicted for temperatures differences ranging between 100 K and 300 K. Shortly afterwards, both experimental and theoretical studies of radiative heat flux modulation with a phase change material, VO_2 for instance, were reported in both the far-field and the near-field [22–25]. Heat flux contrasts up to 80% and 90% were experimentally proven in the far-field [24] and the near-field[25], respectively. Theoretically, a contrast of radiative heat flux of almost 100% is predicted for a bulk plane-plane glass/ VO_2 configuration [22]. We shall here emphasize that these contrasts are only observed around VO_2 metal-insulator transition temperature (67 °C) which strongly restricts their potential practical scope. Dur-

ing the past year, some authors proposed radiative thermal rectifiers based on VO_2 and other phase change materials [26–29].

In this letter, a far-field radiation based thermal rectifier made of selective emitters previously developed for thermo-photovoltaic applications [30–32] is presented. This device rectification ratios stand up the comparison with those reported in literature for radiative thermal rectifiers and comparable temperature differences. Most importantly, its far-field radiation based principle strongly facilitates experimental implementations.

The designed device is composed of two opaque thermal baths 1 and 2 at temperatures T_1 and T_2 , respectively, and exchanging heat through thermal radiation. Ideally, the spectra of the two bodies would perfectly match for a given temperature difference, so the exchanged heat flux is maximal, and perfectly mismatch when the thermal gradient is reversed so the exchanged flux is minimized. In fact, in the case of perfectly matching spectra, radiation emitted by one body at any wavelength is absorbed by the second body while it is completely reflected and returned to the emitter in the case of perfectly mismatching spectra. A perfect one-way heat transmitter, *i.e.* a thermal diode, can then be realized.

2. Model

Figure 1 presents a schematic of the proposed device composed of two parallel planar bodies 1 and 2 separated by a gap of thickness d and characterized by their dielectric functions and temperatures $(\epsilon_1(T_1), T_1)$ and $(\epsilon_2(T_2), T_2)$, respectively. In forward bias, $T_1 = T_h = 500$

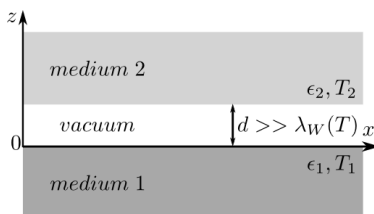


Figure 1: Two parallel planar bodies separated by a distance d . In forward bias configuration, $T_1 = T_h$ and $T_2 = T_c$. In reverse bias configuration, $T_1 = T_c$ and $T_2 = T_h$.

K and $T_2 = T_c = 300$ K. Subscripts h and c stand for hot and cold, respectively. The two bodies temperatures are swapped in reverse bias. These values of T_1 and T_2 are chosen for clarity sake and in order to obtain results comparable to relevant literature [18, 19].

A more detailed discussion of the temperature dependence of the device performances will be presented later for a particular implementation. The net exchanged heat flux densities between 1 and 2 are \dot{q}_{for} and \dot{q}_{rev} in forward and reverse bias, respectively. The rectification coefficient R defined as the relative difference between these two quantities is then given by :

$$R = \frac{\dot{q}_{for} - \dot{q}_{rev}}{\max(\dot{q}_{for}, \dot{q}_{rev})} \quad (1)$$

The two bodies are assumed to be in vacuum. Thus, \dot{q} is a radiative heat flux (RHF) density. The radiative properties of the considered bodies, in particular their emissivities and reflectivities (ε and ρ , respectively), are completely governed by their dielectric functions and geometries. In the case of opaque bodies, energy conservation and Kirchhoff's laws combination leads to the following relation between the monochromatic emissivity and reflectivity at a given temperature:

$$\varepsilon(T, \lambda) = 1 - \rho(T, \lambda) \quad (2)$$

We also assume the two bodies are lambertian sources, thus ε and ρ are direction-independent. The gap width d is assumed to be much larger than the dominant thermal radiation wavelength (Wien wavelength) $\lambda_W(T) = hc/k_B T$ where h , c , k_B and T are Planck's constant, the speed of light in vacuum, Boltzmann's constant and the absolute temperature, respectively. The net RHF density exchanged by the two media reduces then to the far field contribution which can be written [33]:

$$\dot{q}(T_1, T_2) = \pi \int_{\lambda=0}^{\infty} [I^0(\lambda, T_1) - I^0(\lambda, T_2)] \tau(\lambda, T_1, T_2) d\lambda \quad (3)$$

where

$$I^0(\lambda, T) = \frac{2hc}{\lambda^5} \frac{1}{e^{hc/\lambda k_B T} - 1} \quad (4)$$

is the black body intensity at a temperature T and

$$\tau(\lambda, T_1, T_2) = \frac{\varepsilon_1(\lambda, T_1)\varepsilon_2(\lambda, T_2)}{1 - \rho_1(\lambda, T_1)\rho_2(\lambda, T_2)} \quad (5)$$

is the monochromatic RHF density transmission coefficient between 1 and 2 [34, 35]. Now, let us assume the two bodies are selective emitters so that they behave as quasi-monochromatic spectral emitters, *i.e.* they present reflectivity valleys (or emissivity peaks) of the same finite

width $\Delta\lambda$ at given wavelengths, $\lambda_{p,i}, i \in \{1, 2\}$ for instance. Outside the emission peaks, they can be seen as piecewise gray bodies and their reflectivities can be written as follows:

$$\rho_i(\lambda, T) = \begin{cases} \rho_{min}(T) \simeq 0 & \text{if } \lambda \in [\lambda_{p,i}(T) - \Delta\lambda/2, \lambda_{p,i}(T) + \Delta\lambda/2] \\ \rho_{iI}(T) \simeq 1 & \text{if } \lambda < \lambda_{p,i}(T) - \Delta\lambda/2 \\ \rho_{iII}(T) \simeq 1 & \text{if } \lambda > \lambda_{p,i}(T) + \Delta\lambda/2 \end{cases} \quad (6)$$

These reflectivities are illustrated in the insets of Figure 2 for a given set of parameters : $\Delta\lambda = 1 \mu\text{m}$, $\rho_{min} = 10^{-2}$, $\rho_{iI} = \rho_{iII} = 0.99$ and $\lambda_{p,1}(T) = \lambda_W(T_h = 500\text{K})$. Body 1 emissivity is temperature independent. Body 2 emissivity is initially identical to that of body 1 in forward bias ($\lambda_{p,2}(T_c) = \lambda_{p,1}$) while its peak shifts to the red by $\delta_{rev}\lambda_p$ when the temperatures of the two bodies are reversed *i.e.* $\lambda_{p,2}(T_h) = \lambda_{p,1} + \delta_{rev}\lambda_p$. This shift with the temperature of one of the selective emitters emission peak is the key to achieve thermal rectification. In practice, this shift is completely governed by the used materials thermo-optical properties (TOP), *i.e.* $\partial\epsilon'/\partial T$ and $\partial\epsilon''/\partial T$ where ϵ' and ϵ'' are the real and imaginary part of the material dielectric permittivity, respectively. Now, consider a small shift verifying $\delta_{rev}\lambda_p < \Delta\lambda$ thus the two peaks still partially overlap in reverse biased configuration. The transmission coefficient resulting from this emissivities choice for both configurations is plotted in Figure 2. We can then note a one- μm wide spectral transmission window of RHF in forward bias and a narrower window in reverse bias. This asymmetry when the temperatures of the two bodies are inverted would lead to a thermal rectification. In fact, the exchanged RHF in forward bias is given by :

$$\begin{aligned} \dot{q}_{for} \simeq & \sigma T_h^4 [F_{\lambda_{p,1}+\Delta\lambda/2}(T_h) - F_{\lambda_{p,1}-\Delta\lambda/2}(T_h)] \\ & - \sigma T_c^4 [F_{\lambda_{p,1}+\Delta\lambda/2}(T_c) - F_{\lambda_{p,1}-\Delta\lambda/2}(T_c)] \\ & + \pi \int_{\lambda \in \mathcal{L}_{for}} \frac{\epsilon_1(\lambda, T_h)\epsilon_2(\lambda, T_c)}{1 - \rho_1(\lambda, T_h)\rho_2(\lambda, T_c)} [I^0(\lambda, T_h) - I^0(\lambda, T_c)] \end{aligned} \quad (7)$$

where σ is Stefan-Boltzmann constant and

$$\sigma T^4 = \pi \int_0^\infty I^0(\lambda', T) d\lambda' \quad (8)$$

is the emissive power of a black body at a temperature T. The spectral fraction of black body radiation emitted in the spectral range $\lambda' \leq \lambda$ and $\mathcal{L}_{for} = [0, \lambda_{p,1} - \Delta\lambda/2] \cup [\lambda_{p,1} +$

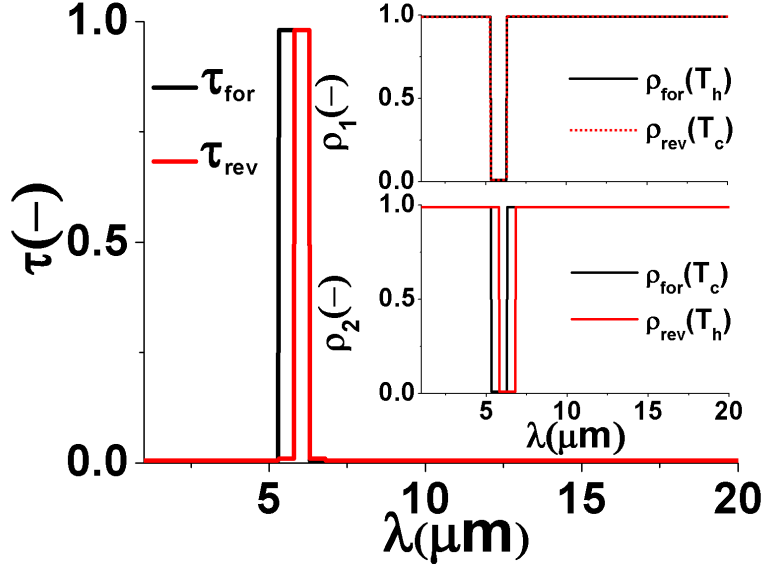


Figure 2: The transmission coefficient in forward and reverse biased configurations and bodies 1 and 2 reflectivities in forward (top inset) and reverse bias (bottom inset) configurations. In both configurations, $\lambda_{p,1}(T) = \lambda_W(T_h) = 5.8 \mu\text{m}$ while $\lambda_{p,2}(T_c) = \lambda_{p,1}$ in forward bias and $\lambda_{p,2}(T_h) = \lambda_{p,1} + \delta_{rev}\lambda_p$ in reverse bias where $\delta_{rev}\lambda_p = \Delta\lambda/2$.

$\Delta\lambda/2, \infty]$ is

$$F_\lambda(T) = \pi \frac{\int_0^\lambda I^0(\lambda', T) d\lambda'}{\sigma T^4} \quad (9)$$

On the other hand, the exchanged RHF in reverse bias is given by :

$$\begin{aligned} \dot{q}_{rev} \simeq & \sigma T_h^4 [F_{\lambda_{p,1} + \Delta\lambda/2}(T_h) - F_{\lambda_{p,1} + \delta_{rev}\lambda_p - \Delta\lambda/2}(T_h)] \\ & - \sigma T_c^4 [F_{\lambda_{p,1} + \Delta\lambda/2}(T_c) - F_{\lambda_{p,1} + \delta_{rev}\lambda_p - \Delta\lambda/2}(T_c)] \\ & + \pi \int_{\lambda \in \mathcal{L}_{rev}} \frac{\varepsilon_1(\lambda, T_c)\varepsilon_2(\lambda, T_h)}{1 - \rho_1(\lambda, T_c)\rho_2(\lambda, T_h)} [I^0(\lambda, T_h) - I^0(\lambda, T_c)] \end{aligned} \quad (10)$$

where $\mathcal{L}_{rev} = [0, \lambda_{p,1} + \delta_{rev}\lambda_p - \Delta\lambda/2] \cup [\lambda_{p,1} + \Delta\lambda/2, \infty]$.

The piecewise decompositions of the exchanged RHF in Eqs. 7 and 10 take into account the fact that $\varepsilon_i \simeq 1$ within the structure i peak. Since $\varepsilon_i \simeq 0$ elsewhere else, the terms with the pre-factor $\varepsilon_1\varepsilon_2/(1 - \rho_1\rho_2)$ in the integrand are of the first order. In reverse biased configuration, we can note that the spectral domains of the zeroth and the first order terms are

reduced and extended, respectively, due to the shift between the two peaks. The reduction of the dominating term (order 0) due to its spectral domain diminution, if it is different from the higher order term (1st order) increase, would lead to an asymmetry of the RHF and therefore a rectification phenomenon. For the above presented situation, calculations lead to: $\dot{q}_{for} = 122.67 \text{ W.m}^{-2}$, $\dot{q}_{rev} = 63.97 \text{ W.m}^{-2}$ and $R = 0.48$. This rectification value is of the order of the largest reported values for radiative thermal rectifiers.

According to the previous assumptions, this rectification ratio obviously depends on the chosen parameters, in particular the temperatures T_h and T_c , the peaks position λ_p compared to $\lambda_W(T_h)$, their width $\Delta\lambda$ compared to the black body spectrum useful width at the largest temperature, the shift between the two peaks in reverse bias $\delta_{rev}\lambda_p$ compared to $\Delta\lambda$ and the reflectors and emitters quality characterized by ρ_{ij} and ρ_{min} , respectively. It is clear that the maximal rectification ratio is reached when the peaks shift in reverse bias is larger than the peaks width and when the bodies are perfect reflectors outside the peaks, *i.e.* when $\delta_{rev}\lambda_p/\Delta\lambda \geq 1$ and $\rho_{ij} = 1$, respectively : reverse bias RHF vanishes and rectification reaches 1. The first condition on $\delta_{rev}\lambda_p$ is more easily realized with narrow emissivity peaks. However, narrower emissivity peaks would decrease forward bias RHF density which makes the rectification ratio more sensitive to the RHF density noise (high order terms), *i.e.* to heat transmitted in a spectral range outside the peaks thus to ρ_{ij} . Besides, since ρ_{ij} and ρ_{min} are temperature dependent, other behaviors may be observed if these parameters actually vary when the temperature gradient is reversed. An increase of ρ_{ij} in reverse bias for instance, even small, would induce a supplementary exchanged RHF. This supplementary RHF may counterbalance or overcome the flux decrease due to the peaks shift. The final rectification is then a balance between the two phenomena.

3. Implementation

Now, we propose an implementation of the above presented device concept. The key point to obtain such a rectification device is to use selective emitters, *i.e.* bodies that behave as mirrors in the mid-infrared except in a narrow-band wavelength range where they strongly emit, with sufficiently different TOP. For this purpose, we use selective emitters based on Fabry-Pérot resonant cavities previously developed for thermo-photovoltaic applications [31]. First, these structures present emissivity peaks in the near and mid infrared. Second, the

peaks positions and widths can be controlled by few simple parameters such as the layers thicknesses and the quality of the cavity reflectors. Finally, a former fine analysis of these structures TOP [36] showed that they fulfill the required conditions to observe the radiative thermal rectification phenomenon.

Consider the system presented in Figure 3. The interacting bodies are two Fabry-Pérot

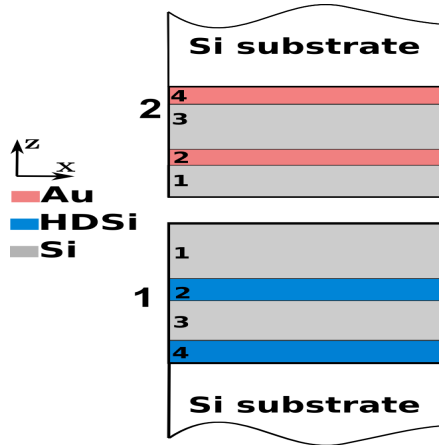


Figure 3: A radiative thermal rectification device based on two Fabry-Pérot cavities. The reflectors of body 1 are made of *p*-type heavily doped silicon (HDSi) at $N = 3.8 \times 10^{20} \text{ cm}^{-3}$ while those of body 2 are made of gold (Au). The transparent layers and the substrates are made of intrinsic silicon. The dimensions of the different layers in nanometer are $d_{1,1} = 320$, $d_{1,2} = 10$, $d_{1,3} = 360$ and $d_{1,4} = 22$ for body 1, and $d_{2,1} = 95$, $d_{2,2} = 10$, $d_{2,3} = 370$, $d_{2,4} = 420$ for body 2. In forward bias $T_1 = T_h$ and $T_2 = T_c$. In reverse bias, the two bodies temperatures are inverted.

cavities made of four thin films alternating a transparent and a reflecting film on a thick intrinsic silicon substrate. Transparent layers are made of intrinsic silicon. Reflectors are made of *p*-type heavily doped silicon (HDSi) in one case, and gold (Au) in the other. Gold and heavily doped silicon dielectric functions at considered temperatures are given by Drude models (see appendix A). We assume the system geometry unchanged in the considered temperature range. In fact, the linear thermal expansion coefficient of used materials is, at the most, of the order of 10^{-5} K^{-1} . This leads, for a 100 K temperature variation, to a relative variation of the films thicknesses of one thousandth. Such a variation has no significant impact on the radiative properties of the considered structures [36]. However, when it comes to a practical realization, a second geometrical effect should be taken into

account. Indeed, the finite dimensions of the system affect the exchanged fluxes given by Equation 10. In this expression, a unit view factor between the two bodies is assumed while it is lower than one for finite size samples. For instance, if we consider two identical 20-mm side squares separated by a 1-mm wide gap, the view factors are identical $F_{12} = F_{21} = 0.9$. Multiplying Equation 10 terms by the view factors and the bodies surfaces areas allows a more accurate prediction of exchanged RHF [33]. Rectification ratio is not affected though since surface areas and view factors cancel out in Equation 1.

The reflectivities of Figure 3 structures at normal incidence at $T_c = 300$ K and $T_h = 500$ K calculated by the transfer matrix method are presented in the inset of Figure 4. Only normal reflectivity is plotted since these structures show isotropic radiative properties [31]. **We remind here that the optical properties of Fabry-Pérot cavities are not isotropic in general as shown in Ref. [30, 32]. In these works, the cavities were made of three thin films : two reflectors surrounding a transparent layer. In the present work, the resonator is made of four thin films. The supplementary film (layer 1) is deposited on the first reflector and is necessary to insure the optical properties isotropy. A high contrast between this coating and the surrounding medium, vacuum in this case, refractive indices is needed for this purpose. In the case of Figure 3, the coating is made of silicon with a refractive index $n_{Si} = 3.42$ in the considered wavelength range (Appendix A). Consequently, incident radiation from the whole light cone in vacuum is collimated within a much narrower cone in the silicon coating layer with an angular width $\Delta\theta = \arcsin(1/n_{Si}) = 17^\circ$. Consequently, all incident radiation impinges on the Fabry-Pérot cavity with almost normal incidence which leads to isotropic optical properties.** The inset of Figure 4 shows that Si/Au structure reflectivity exhibits a more pronounced variation with temperature than Si/HDSi cavity. The impact of this temperature dependence on the exchanged RHF can be deduced from the plot of the spectral transmission coefficient τ in Figure 4. In both configurations, τ exhibits two peaks corresponding to the first and second order modes of the Fabry-Pérot cavities. In reverse bias configuration, both peaks positions and magnitudes slightly shift and increase, respectively, with a more pronounced increase for the second order peak magnitude though. Indeed, the area under this peak increases by more than 50%. Besides, Au/Si structure reflectivity over the whole spectrum slightly decreases which induces an increase of its absorptivity over a wide spectral range. All these

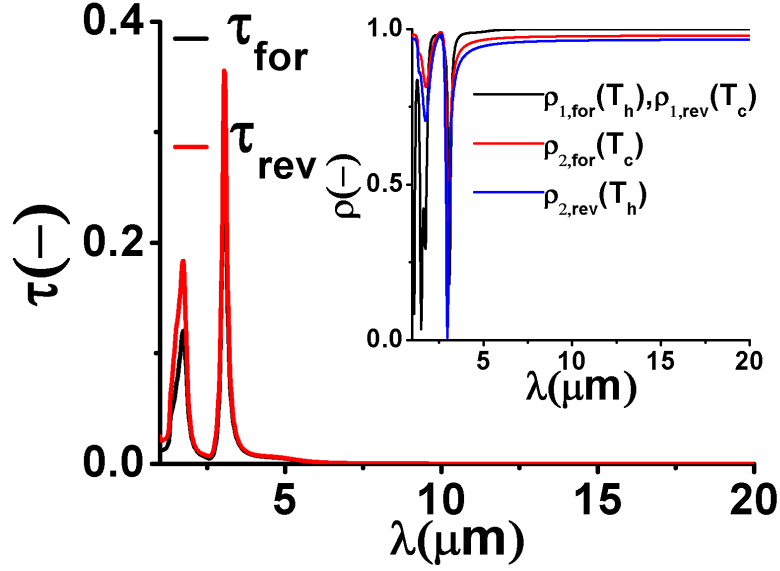


Figure 4: Spectral transmission coefficient of the device presented in Figure 3 in forward (τ_{for} in black) and reverse bias (τ_{rev} in red) configurations. The inset shows the reflectivity of the two bodies in both configurations. In black, the reflectivity of body 1 at T_h and T_c which is temperature independent. For body 2, in red and blue the reflectivity at T_c (forward) and T_h (reverse) respectively.

evolutions would obviously induce an increase in the net RHF. A numerical application leads to a rectification ratio $R = -0.08$.

The proposed device rectification is therefore of 8% for $\Delta T = 200$ K. Rectification goes up to 19% for $\Delta T = 370$ K. Figure 5 presents the evolution of R as a function of ΔT in the temperature range where the used materials TOP data are available, up to $\Delta T = 370$ K in this case. The modeling of the temperature dependence of the used materials infrared optical properties is presented in appendix A. However, instead of diminishing as described for the ideal device, the net RHF density increases when switching from forward to reverse bias configurations. This is mainly due to the fact that gold TOP are not sufficiently large to induce a significant shift of Au/Si structure emissivity peak. Note that the proposed device can be improved to obtain higher rectification since several parameters affect the system performances, which certainly calls a detailed parametric study.

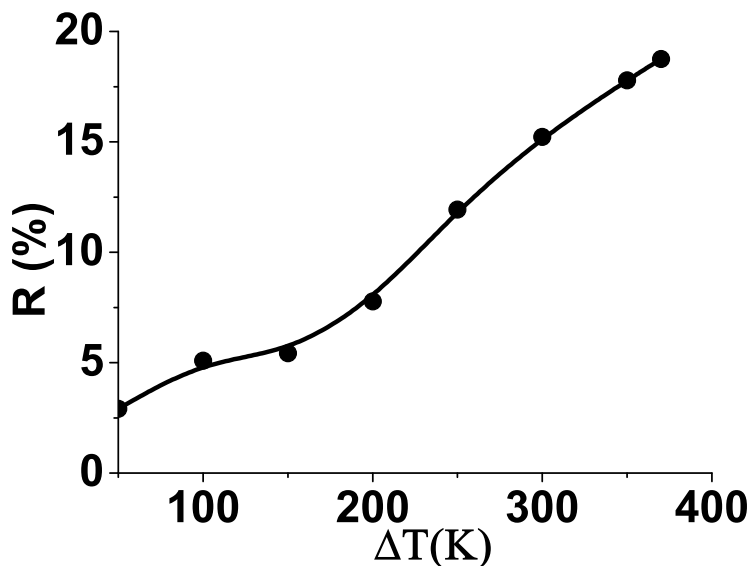


Figure 5: Rectification coefficient as a function of the two bodies temperature difference ΔT

4. Conclusion

Thermal rectification currently drives a growing attention because of its huge potential applications. Surprisingly, few radiation based rectifiers, mostly based on near-field thermal radiation, have been reported thus far. The use of near-field effects makes those devices out of reach of current experimental setups since they require the alignment of planar bodies separated by nanometric vacuum gaps. In this letter, we presented the first theoretical concept of a thermal rectifier based on far-field thermal radiation. Then, we suggested a real nano-structured system based on two multi-layered bodies as a candidate for an experimental observation. The consideration of far-field radiation shall allow straightforward experimental implementations. Beside its experimental affordability, this system shows an absolute rectification value of the order of the highest reported in literature with near-field radiative devices. In addition and since it is based on spectrally tunable selective emitters, the presented rectifier can be configured to operate in different spectral ranges and temperatures and leaves undoubted room for improvement. Indeed, all what have been realized so far on the design and optimization of photonic devices can be extended to manage heat fluxes if the thermal dependence of photonic structures optical properties is controlled.

Presented results might be useful for thermal management applications and pave the way to the development of thermal logical circuits.

Appendix A: Materials thermo-optical properties

The temperature dependence of the materials optical properties is a key point in the radiative thermal diode device we propose. This appendix details the modeling of the temperature dependence we used in our calculations for gold, heavily doped silicon and intrinsic silicon optical properties.

1. Gold

Gold (Au) dielectric function in the infrared can be modeled by a Drude model[37, 38].

$$\epsilon(\omega) = 1 - \frac{\omega_p^2}{\omega(\omega + i\Gamma)} \quad (\text{A1})$$

where $\omega = 2\pi c/\lambda$ is the circular frequency, ω_p is the plasma frequency and Γ is the damping coefficient. The values of ω_p and Γ for different temperatures are given in table 1[37] for the spectral range 1 – 30 μm . The different parameters of table 1 are related by [39]:

T	σ_0	τ	ω_p	Γ
(K)	(10^{17} s^{-1})	(10^{14} s)	(10^{16} s^{-1})	(10^{13} s^{-1})
295	3.79	2.4	1.4087	4.1667
300*	3.75	2.4	1.4099	4.2517
470	2.35	1.4	1.4524	7.1429
500*	2.23	1.3	1.4502	7.634
670	1.58	0.96	1.4381	10.417

Table 1: Drude model parameters for gold at different temperatures. The values of σ_0 (steady-state electrical conductivity) and τ (free electron relaxation time) are retrieved from literature[37] while those of ω_p and Γ are obtained through expressions A2 and A3.

* : values are obtained by a linear interpolation (not from Ref[37].)

$$\omega_p^2 = 4\pi \frac{\sigma_0}{\tau} \quad (\text{A2})$$

and

$$\Gamma = \frac{1}{\tau} \quad (\text{A3})$$

2. Heavily doped silicon

Heavily doped silicon dielectric function can also be modeled by a Drude model [40, 41]:

$$\epsilon(\omega) = \epsilon_\infty - \frac{\omega_p^2}{\omega(\omega + i\Gamma)} \quad (\text{A4})$$

where $\epsilon_\infty = 11.7$ is the high frequency limit of the dielectric function. ω_p and Γ are given by :

$$\omega_p^2 = \frac{Ne^2}{(m^*\epsilon_0)} \quad (\text{A5})$$

and

$$\Gamma = \frac{1}{\tau} = \frac{e}{m^*\mu} \quad (\text{A6})$$

where ϵ_0 is the vacuum permittivity. τ , μ et m^* are the relaxation time, mobility and effective mass of carriers (electrons / holes), respectively, which depend on the carriers density N and temperature [40–43]. At the considered doping level, we assume complete impurity ionization. The mobility of electrons and holes of phosphorus doped silicon as a function of carriers concentration and temperature is given by[42] :

$$\mu_e = 88 T_n^{-0.57} + \frac{7.4 \times 10^8 T^{-2.33}}{1 + [N/(1.26 \times 10^{17} T_n^{2.4})]0.88 T_n^{-0.146}} \quad (\text{A7})$$

for electrons and

$$\mu_h = 54.3 T_n^{-0.57} + \frac{1.36 \times 10^8 T^{-2.23}}{1 + [N/(2.35 \times 10^{17} T_n^{2.4})]0.88 T_n^{-0.146}} \quad (\text{A8})$$

for holes where $T_n = T/300$ denotes the reduced temperature. These expressions show a very good agreement with experimental values up to $N = 10^{20} \text{ cm}^{-3}$.

The effective mass of electrons at room temperature is given by $m^* = 0.27m_0$ and $m^* = 0.34m_0$ for n -type and p -type doped silicon, respectively, where $m_0 = 9.1 \times 10^{-31} \text{ Kg}$ denotes the free electron mass in vacuum [40]. The effective mass varies very slightly with temperature [43–45]. It is therefore considered temperature independent in this study. According to the given model and assumptions, the damping coefficient increases by almost 30% (Table 2) while the plasma frequency remains constant in the considered temperature range.

T (K)	300	500
μ (cm ² /V.s)	55.38	41.84
Γ (10 ¹² s ⁻¹)	5.26	6.96

Table 2: Carriers mobility and damping coefficient for p -type doped silicon at $N = 10^{20}$ (cm⁻³) at $T = 300$ K and $T = 500$ K.

3. Intrinsic silicon

Intrinsic silicon refractive index n is assumed to be constant in the considered temperature range [46, 47] ($n = 3.42$). As a matter of fact, its value for slightly doped silicon at different temperatures is presented in table 3 and shows very small variations.

Doping type	T (K)	n
p	331	3.3
p	547	3.4
n	293	3.43
n	543	3.48

Table 3: Mean values of p and n -type slightly doped silicon refractive index n in the spectral range $[1, 6]$ μm at $T = 300$ K and $T = 500$ K.

Acknowledgments

Authors gratefully acknowledge the support of the Agence Nationale de la Recherche through the Source-TPV Project No. ANR 2010 BLAN 0928 01. This work pertains to the French Government program ‘‘Investissements d’Avenir’’ (LABEX INTERACTIFS, reference ANR-11-LABX-0017-01).

References

- [1] L. Wang and B. Li. Phononics gets hot. *Phys. World*, 21:27–29, 2008.

- [2] C.W. Chang, D. Okawa, A. Majumdar, and A. Zettl. Solid-state thermal rectifier. *Science*, 314(5802):1121–1124, 2006.
- [3] R. Scheibner, M. König, D. Reuter, A. D. Wieck, C. Gould, H. Buhmann, and L. W. Molenkamp. Quantum dot as thermal rectifier. *New J. Phys.*, 10(8):083016, 2008.
- [4] W. Kobayashi, Y. Teraoka, and I. Terasaki. An oxide thermal rectifier. *Appl. Phys. Lett.*, 95(17):171905, 2009.
- [5] M. Terraneo, M. Peyrard, and G. Casati. Controlling the energy flow in nonlinear lattices: A model for a thermal rectifier. *Phys. Rev. Lett.*, 88:094302, Feb 2002.
- [6] B. Li, L. Wang, and G. Casati. Thermal diode: Rectification of heat flux. *Phys. Rev. Lett.*, 93:184301, Oct 2004.
- [7] B. Li, J. Lan, and L. Wang. Interface thermal resistance between dissimilar anharmonic lattices. *Phys. Rev. Lett.*, 95:104302, Sep 2005.
- [8] B. Hu, L. Yang, and Y. Zhang. Asymmetric heat conduction in nonlinear lattices. *Phys. Rev. Lett.*, 97:124302, Sep 2006.
- [9] J. Hu, X. Ruan, and Y. P. Chen. Thermal conductivity and thermal rectification in graphene nanoribbons: A molecular dynamics study. *Nano Lett.*, 9(7):2730–2735, 2009.
- [10] N. Yang, G. Zhang, and B. Li. Thermal rectification in asymmetric graphene ribbons. *Appl. Phys. Lett.*, 95(3):033107, 2009.
- [11] D. Segal. Single mode heat rectifier: Controlling energy flow between electronic conductors. *Phys. Rev. Lett.*, 100:105901, Mar 2008.
- [12] N. Yang, N. Li, L. Wang, and B. Li. Thermal rectification and negative differential thermal resistance in lattices with mass gradient. *Phys. Rev. B*, 76:020301, Jul 2007.
- [13] L. Wang and B. Li. Thermal logic gates: Computation with phonons. *Phys. Rev. Lett.*, 99:177208, Oct 2007.
- [14] W. C. Lo, L. Wang, and B. Li. Thermal transistor: Heat flux switching and modulating. *J. Phys. Soc. Jpn.*, 77(5):054402, 2008.
- [15] N. Li, J. Ren, L. Wang, G. Zhang, P. Hänggi, and B. Li. *Colloquium* : Phononics: Manipulating heat flow with electronic analogs and beyond. *Rev. Mod. Phys.*, 84:1045–1066, Jul 2012.
- [16] N.A. Roberts and D.G. Walker. A review of thermal rectification observations and models in solid materials. *Int. J. Therm. Sci.*, 50(5):648 – 662, 2011.

- [17] T. Ruokola, T. Ojanen, and A-P. Jauho. Thermal rectification in nonlinear quantum circuits. *Phys. Rev. B*, 79:144306, Apr 2009.
- [18] C. R. Otey, W. T. Lau, and S. Fan. Thermal rectification through vacuum. *Phys. Rev. Lett.*, 104:154301, Apr 2010.
- [19] S. Basu and M. Francoeur. Near-field radiative transfer based thermal rectification using doped silicon. *Appl. Phys. Lett.*, 98(11):113106, 2011.
- [20] L. P. Wang and Z. M. Zhang. Thermal rectification enabled by near-field radiative heat transfer between intrinsic silicon and a dissimilar material. *Nanoscale Microscale Thermophys. Eng.*, 17(4):337–348, 2013.
- [21] L. Zhu, C. R. Otey, and S. Fan. Ultrahigh-contrast and large-bandwidth thermal rectification in near-field electromagnetic thermal transfer between nanoparticles. *Phys. Rev. B*, 88:184301, Nov 2013.
- [22] P. J. van Zwol, K. Joulain, P. Ben Abdallah, J. J. Greffet, and J. Chevrier. Fast nanoscale heat-flux modulation with phase-change materials. *Phys. Rev. B*, 83:201404, May 2011.
- [23] P. J. van Zwol, K. Joulain, P. Ben-Abdallah, and J. Chevrier. Phonon polaritons enhance near-field thermal transfer across the phase transition of VO_2 . *Phys. Rev. B*, 84:161413, Oct 2011.
- [24] P. J. van Zwol, L. Ranno, and J. Chevrier. Emissivity measurements with an atomic force microscope. *Journal of Applied Physics*, 111(6):063110, 2012.
- [25] P. J. van Zwol, L. Ranno, and J. Chevrier. Tuning near field radiative heat flux through surface excitations with a metal insulator transition. *Phys. Rev. Lett.*, 108:234301, Jun 2012.
- [26] Ph. Ben-Abdallah and S-A. Biehs. Phase-change radiative thermal diode. *Appl. Phys. Lett.*, 103(19):–, 2013.
- [27] J. Huang, Q. Li, Z. Zheng, and Y. Xuan. Thermal rectification based on thermochromic materials. *Int. J. Heat Mass Transfer*, 67(0):575 – 580, 2013.
- [28] Y. Yang, S. Basu, and L. Wang. Radiation-based near-field thermal rectification with phase transition materials. *Appl. Phys. Lett.*, 103(16):–, 2013.
- [29] E. Nefzaoui, K. Joulain, J. Drevillon, and Y. Ezzahri. Radiative thermal rectification using superconducting materials. *Appl. Phys. Lett.*, 104(10):–, 2014.
- [30] L.P. Wang, B.J. Lee, X.J. Wang, and Z.M. Zhang. Spatial and temporal coherence of thermal radiation in asymmetric fabry–perot resonance cavities. *International Journal of Heat and*

- Mass Transfer*, 52(13–14):3024 – 3031, 2009.
- [31] E. Nefzaoui, J. Drevillon, and K. Joulain. Selective emitters design and optimization for thermophotovoltaic applications. *J. Appl. Phys.*, 111(8):084316, 2012.
- [32] S. Shu, Z. Li, and Y. Y. Li. Triple-layer fabry-perot absorber with near-perfect absorption in visible and near-infrared regime. *Opt. Express*, 21(21):25307–25315, Oct 2013.
- [33] M. F. Modest. *Radiative Heat Transfer*. McGraw-Hill, 1993.
- [34] Ph. Ben-Abdallah and K. Joulain. Fundamental limits for noncontact transfers between two bodies. *Phys. Rev. B*, 82:121419, Sep 2010.
- [35] S.-A. Biehs, E. Rousseau, and J.-J. Greffet. Mesoscopic description of radiative heat transfer at the nanoscale. *Phys. Rev. Lett.*, 105:234301, Dec 2010.
- [36] E. Nefzaoui. *Conception et optimisation d'émetteurs sélectifs pour applications thermophotovoltaïques*. PhD thesis, Université de Poitiers, 2013.
- [37] G. P. Pells and M. Shiga. The optical properties of copper and gold as a function of temperature. *J. Phys. C Solid State*, 2(10):1835, 1969.
- [38] M. Rashidi-Huyeh and B. Palpant. Counterintuitive thermo-optical response of metal-dielectric nanocomposite materials as a result of local electromagnetic field enhancement. *Phys. Rev. B*, 74(7):075405, 2006.
- [39] N.W. Ashcroft and N.D. Mermin. *Solid state physics*. Saunders College, 1976.
- [40] F. Marquier, K. Joulain, J.-P. Mulet, R. Carminati, and J.-J. Greffet. Engineering infrared emission properties of silicon in the near field and the far field. *Opt. Commun.*, 237(4-6):379 – 388, 2004.
- [41] S. Basu, B. J. Lee, and Z. M. Zhang. Near-field radiation calculated with an improved dielectric function model for doped silicon. *J. Heat Trans.*, 132(2):023302, 2010.
- [42] N. D. Arora, J. R. Hauser, and D. J. Roulston. Electron and hole mobilities in silicon as a function of concentration and temperature. *IEEE Trans. Electron Devices*, 29(2):292 – 295, 1982.
- [43] M. A. Green. Intrinsic concentration, effective densities of states, and effective mass in silicon. *J. Appl. Phys.*, 67(6):2944–2954, 1990.
- [44] C. J. Fu and Z. M. Zhang. Nanoscale radiation heat transfer for silicon at different doping levels. *Int. J. Heat Mass Trans.*, 49(9–10):1703 – 1718, 2006.

- [45] W. G. Spitzer and H. Y. Fan. Determination of optical constants and carrier effective mass of semiconductors. *Phys. Rev.*, 106:882–890, Jun 1957.
- [46] N.M. Ravindra, S. Abedrabbo, W. Chen, F.M. Tong, A.K. Nanda, and A.C. Speranza. Temperature-dependent emissivity of silicon-related materials and structures. In *IEEE Trans. Semicond. Manuf.*, volume 11, pages 30–39. AIP, 1998.
- [47] T. Satō. Spectral emissivity of silicon. *Jpn. J. Appl. Phys.*, 6(3):339–347, 1967.